Size Dependent Ultrafast Cooling of Water Droplets in Microemulsions by Picosecond Infrared Spectroscopy

G. Seifert, T. Patzlaff, and H. Graener

Martin-Luther-Universität Halle-Wittenberg, Fachbereich Physik, Hoher Weg 8, D-06099 Halle, Germany

(Received 23 November 2001; published 22 March 2002)

The ultrafast thermal relaxation of reversed micelles in *n*-octane/AOT/water (where AOT denotes sodium di-2-ethylhexyl sulfosuccinate) microemulsions was investigated by time-resolved infrared pump-probe spectroscopy. This picosecond cooling process can be described in terms of heat diffusion, demonstrating a new method to determine the nanometer radii of the water droplets. The reverse micelles are stable against transient temperatures far above the equilibrium stability range. The amphiphilic interface layer (AOT) seems to provide an efficient heat contact between the water and the nonpolar solvent.

DOI: 10.1103/PhysRevLett.88.147402 PACS numbers: 78.47.+p, 82.53.Hn

In a typical water-in-oil microemulsion, water is dispersed in a nonpolar solvent in the form of nanometer-sized spherical droplets coated by a monolayer of surfactant molecules. These so-called reverse micelles have raised considerable interest in the past few years, not least because of their attractivity for a variety of technical applications such as chemical catalysis, drug delivery, or nanocluster synthesis. A large number of experimental and theoretical investigations revealed information about, e.g., the essential role of the surfactant layer for structure and phase behavior [1–6], or dealt with questions such as solvation dynamics both in the water pool and close to the surfactant layer [7–10]. While the structure and dynamics of water in the reverse micelles are strongly modified directly at the interface [6,11], the basic properties of bulk water reemerge within a few molecular layers [6,12]. So, in appropriate ternary mixtures with droplet sizes of at least several nanometers, most of the water in such a microemulsion is found in its bulk configuration.

Recent femtosecond infrared laser experiments revealed that energy dissipation after vibrational excitation in the OH stretching region in neat water happens on a subpicosecond time scale [13–17]. So time-resolved infrared spectroscopy with an appropriate pulse length can be used to selectively heat the water inside reverse micelles within a few picoseconds, and trace the cooling process by monitoring the temperature dependent changes of the OH stretching band, as we demonstrated recently [18]. In this Letter, we report a series of such experiments on octane-AOT-water ternary mixtures (where AOT denotes sodium di-2-ethylhexyl sulfosuccinate). The presented analysis demonstrates a new method to determine the size of the water droplets in microemulsions, and gives evidence that the amphiphilic AOT interface allows for a very efficient transfer of heat from water into the nonpolar solvent. The reverse micelles are found to be stable against quite high transient temperatures, which is very interesting for applications, e.g., as nanoreactors.

The experiments were performed in an IR double resonance spectrometer, as described in detail recently [19], which provides separately tunable pump and probe pulses of 2.5 ps temporal and 8–10 cm^{-1} spectral width (full width at half maximum). The intense pump pulses of typically 25 μJ energy are tuned to the water OH stretching band, creating an ultrafast temperature rise via vibrational excitation and the subsequent subpicosecond relaxation processes [13–17]. The probe pulses (energy <1 μJ) monitor the corresponding transient transmission changes up to a maximum pump-probe time delay of ≈ 3 ns. We will here use only the "rotation-free" transmission change $\Delta\alpha_{\mathrm{rf}} = 1/3[\ln(T_{\parallel}/T_0) + 2\ln(T_{\perp}/T_0)]$ [19], which was originally defined to be directly proportional to excess vibrational population, but turns out to be also directly proportional to the water temperature in certain frequency ranges (see below). Because of this definition, bleaching is represented by positive values of $\Delta\alpha_{\mathrm{rf}}$.

The samples (length 500 μm) used for our investigations were mixtures of *n*-octane, AOT, and water. The surfactant AOT (Aldrich, 98%) and the alkane oil *n*-octane (Merck, water-free grade) were used without further purification. The water was deionized and distilled twice before use. We characterize these microemulsions by the usual parameter molar water-to-AOT ratio $\mu = [H_2O]/[AOT]$ (sometimes referenced as w_0) and water mass fraction $\alpha = m_{\mathrm{water}}/m_{\mathrm{total}}$. While μ determines the size of the reversed micelles (often a simple linear relation assuming a monodisperse size distribution can be used [20]), α is correlated with the micelle concentration at given μ. In this study, we used samples with $\alpha = 0.005$ and $10 < \mu < 55$, i.e., rather large reverse micelles at low concentration. In the IR absorption spectrum, the OH stretching band appears well separated from any resonances of *n*-octane and AOT [18], and has approximately the same shape as in neat water. This confirms that most of the water inside the reverse micelles is in bulk configuration.

A few examples for transient spectra are given in Fig. 1, which were obtained on a sample with $\mu = 20$ at different delay times of 10 (squares), 150 (circles), and 1000 ps (triangles) after vibrational excitation at 3400 cm^{-1}; for comparison, the dashed line shows an arbitrarily scaled

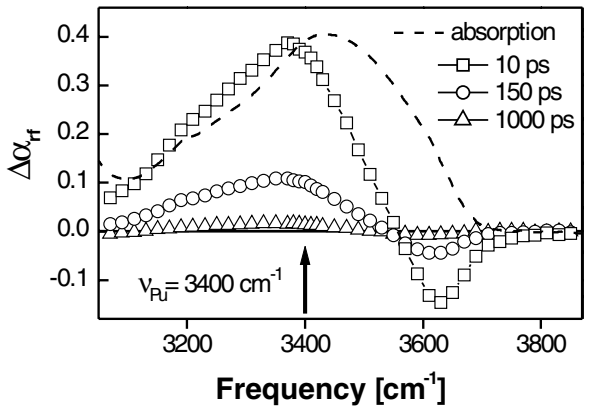

FIG. 1. Transient spectral changes of an n-octane/AOT/water microemulsion ($\mu = 20, \alpha = 0.005$) at different delay times (10, 150, and 1000 ps) after excitation at 3400 cm^{-1}. Dashed line: conventional IR absorption of the sample (scaled).

conventional (water) absorption spectrum of the sample. At all three times, very similar spectral shapes are found, namely, bleaching from 3100 to 3550 cm^{-1} and absorption increase between 3550 and 3800 cm^{-1}. As a function of time, the amplitude decreases, but the spectral shape remains nearly constant. As the excess OH vibrational energy in pure water is thermalized within a few picoseconds [13–17], the observed spectral changes can be due only to the elevated temperature within the micelle. The corresponding rearrangement and, on average, weakening of the hydrogen bonds leads to a blueshift of the OH stretching band connected with decreasing integral absorption strength. This well-known behavior explains also the asymmetry of the transient spectra. By studying conventional infrared absorption as a function of sample temperature, difference spectra were obtained very similar to the spectral changes observed after ultrafast laser heating. Evaluating them as a function of temperature difference reveals that, in accordance with previous IR studies [21,22], a linear temperature dependence of the bleaching amplitude is a very good approximation in a frequency interval between 3150 and 3350 cm^{-1}; i.e., transmission changes measured in that spectral range are directly proportional to temperature changes. This is valid already during the excitation process, since the applied pulse duration is clearly longer than vibrational and thermal relaxation in neat water. Consequently, we can assume that the whole excess energy is equilibrated quasi-instantaneously within the water, leading to an increased droplet temperature ($\Delta T_{\max} \approx 40$ K for the data of Fig. 1) after termination of the pump pulse.

Heat transfer out of the water droplet into the (cold) surroundings can be described by the basic laws of heat conduction. A temperature gradient ∇T in a medium with thermal conductivity λ causes a heat flux $\vec{j} = -\lambda \nabla T$. Considering a heat flux in and out of a volume element dV, the exchange rate of thermal energy Q is given by $\nabla \vec{j} dV = -\dot{Q}$. In order to test if these macroscopic laws are applicable to our transient data, we first analyze the homogeneous case (constant, temperature independent λ within the whole system), neglecting any source terms. Then the basic formulas can be combined, leading to the well-known heat equation, which for radial symmetry can be written as

$$\frac{\partial T(r,t)}{\partial t} = \frac{\chi}{r} \frac{\partial^2 [rT(r,t)]}{\partial r^2}, \tag{1}$$

where the parameter $\chi = \lambda / c\rho$ is the thermal diffusivity (c is specific heat and ρ is density). For typical liquids, the values of χ vary only within a range of a factor of 2 [e.g., 0.073 (CCl_4) ... 0.146(H_2O) nm^2/ps]. A hot droplet in cold surroundings can be described by an initial spherical temperature distribution $T(t = 0) = T_{\max}$ for $r \le R$ and $T(t = 0) = 0$ for $r > R$, where T is the temperature difference with respect to the situation before heating, and R denotes the radius of the hot sphere. For this case, Eq. (1) can be solved analytically, yielding the following expression for the temperature T at time t and radial coordinate r:

$$T(t,r,R) = T_{\max} \times \left[\frac{1}{r} \sqrt{\frac{\chi t}{\pi}} [\exp(\xi_+^2) - \exp(\xi_-^2)] + \frac{1}{2} [\mathrm{erf}(\xi_+) + \mathrm{erf}(\xi_-)] \right], \tag{2}$$

where $\xi_\pm(t,r,R) = (R \pm r)/(2\sqrt{\chi t})$. Here erf($x$) denotes the Gaussian error function. It is important to notice that the initial temperature rise $T_{\max}$ is only an amplitude factor. In the experiments, an average temperature change of the water droplet is measured, which is easily calculated by

$$T(t,R) = \frac{3}{R^3} \int_0^R r^2 T(t,r,R)\, dr\,. \tag{3}$$

Figure 2 gives examples of the time evolution of this quantity for three different radii R (7, 10, and 13 nm). A thermal diffusivity of $\chi = 0.1$ nm^2/ps was chosen, which

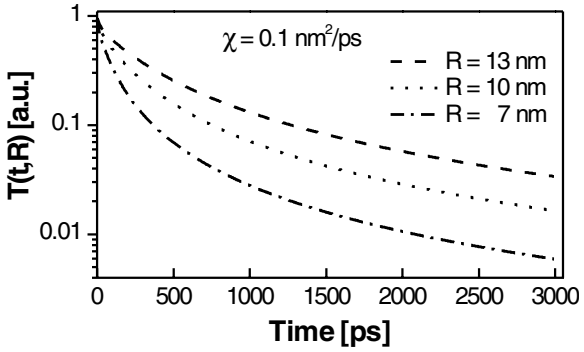

FIG. 2. Calculated time evolution of average droplet temperature $T(t,R)$ of an initially hot sphere for different sphere radii R.

is a typical value for usual fluids. The semilogarithmic plot clearly shows a nonexponential temperature relaxation, and obviously the cooling velocity depends strongly on the radius of the initial hot sphere. The individual decays can be characterized by the parameter $R^2/(4\chi)$ [compare Eq. (2)], which has the dimension of a time; e.g., for the $R = 10$ nm case shown above, a value of 250 ps is obtained. To check for the influence of size dispersion, individual time profiles obtained by Eq. (3) were averaged using reasonable size distributions. The result for a symmetric (Gaussian) distribution with a polydispersity up to 30% (typical value for AOT micelles is 10%) cannot be distinguished from the temperature decay calculated for the average radius. So only the latter will be discussed in the following. For a comparison with experimental data, however, the different thermal diffusivities of water ($\chi = 0.146$ nm^2/ps) and octane ($\chi = 0.082$ nm^2/ps), as well as the possible influence of the AOT shell, have to be considered. These aspects can simply be treated in a numerical simulation of heat transfer based on the above given basic laws, considering the heat fluxes through interfaces of shells of identical (infinitesimal) thickness. Using this method, $T(t, R)$ can be calculated for any $\chi(r, T)$; also, the initial heating process can easily be included.

Figure 3 shows that already a two component model of a water sphere in octane using the room temperature χ values provides a very good description: The different symbols represent time-resolved measurements (excitation at 3300 cm^{-1}, probe frequency 3200 cm^{-1}) in samples with different μ between 20 and 50, while the solid lines give the corresponding best fit curves obtained by the numerical model. Overall the fit quality is very good. Slight deviations between experimental data and calculated curves found at later delay times are attributed to the single droplet assumption implicitly made in the simulations; in reality, at later times, the superposition of the individual temperature profiles of neighboring micelles may become important. The short time behavior, i.e., mainly the signal increase due to the heating process, is shown in the inset of Fig. 3; this increase can very well be described by the integral over the pump pulse convoluted with the probe pulse, as was expected considering the subpicosecond relaxation processes in water. The only variable parameter in the simulations was the radius of the water droplet (called thermodynamic radius R_{th} in the following), the best fit values of which are given in the legend of Fig. 3. So obviously the time evolution of the observed transmission changes (and thus the droplet temperature) is completely governed by the size of the initial temperature distribution.

The radii obtained from our experiments can be compared with the results of other established methods to determine the size of reverse micelles. In particular, Fig. 4 shows, as a function of the water-to-AOT ratio μ, our thermodynamic radii R_{th} (solid circles), the hydrodynamic radii R_h derived from dynamic light scattering experiments [18] (open circles), and the result of a geometrical estimation [20] (solid line). The latter is done simply by comparing the volume and the surface of the water droplet giving a radius $R_g = 3\mu V_{\text{water}}/A_{\text{AOT}}$. Using literature values for the molecular volume of water ($V_{\text{water}} = 0.03$ nm^3) and the effective head group area of a single AOT molecule ($A_{\text{AOT}} = 0.6$ nm^2) [20], this yields the linear dependence $R_g[\text{nm}] = 0.15 \times \mu$; since A_{AOT} decreases for small micelles, this simple relation is valid only for $\mu \geq 15$. All three types of radii show the same principal variation (linear increase with μ), but different values in the order $R_h > R_{\text{th}} > R_g$. It is reasonable that the hydrodynamic radius is the largest one, because R_h describes the whole micelle including the AOT shell, while the other two methods refer to the water droplet alone. The difference between R_{th} and R_g, however, can be explained only partially by the uncertainty of the geometrical parameters. So possible reasons for this discrepancy have to be discussed.

The first important point is the rather large initial temperature rise of $\Delta T_{\text{max}} \approx 75$ K estimated for the data of

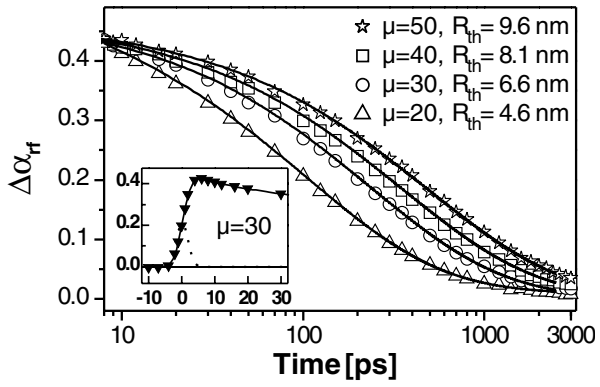

FIG. 3. Time-resolved transmission change measured at $\nu_{\text{pu}} = 3300$ cm^{-1}, $\nu_{\text{pr}} = 3200$ cm^{-1} for different μ. Experimental points, calculated curves (see text for details). Inset: example for signal rise.

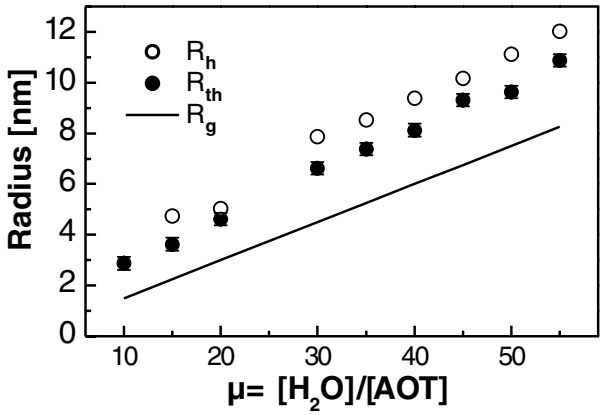

FIG. 4. Thermodynamic (R_{th}, solid circles), hydrodynamic (R_h, open circles), and geometrically estimated (R_g, solid line) water droplet radii as a function of μ.

Fig. 3. This value, in context with the shot-to-shot reversibility of the observed spectral changes, clearly shows that in our experiments the reverse micelles remain stable in spite of transient temperatures at which they would be destroyed in thermal equilibrium [1]. This promises interesting new applications for using reverse micelles as nanoreactors. For the present discussion, it is important to note that during the whole cooling process the system is not in its thermodynamic equilibrium, because thermal and density relaxation of the focal volume (length scale 50 μm) occur on much slower time scales [23]. For example, the thermalization parameter $R^2/4\chi$ gives 45 ms for $R = 50$ μm. This, in principle, discourages the use of equilibrium parameters to account for the temperature variation of χ in the simulations. Doing it nonetheless, the obtained values of R_{th} decrease slightly by $\leq 5\%$ for any of the data shown, while first experiments applying smaller initial temperature increases indicate a larger decrease. This might explain the difference of R_{th} and R_g; but also additional effects such as shock waves and consecutive shape changes have to be considered. Many more extensive studies, which are beyond the scope of this first report, will be necessary to clear these questions in detail. Another important question is the role of the AOT layer, which was neglected until now. For this purpose, we included a layer of 1.0 nm (approximate length of an AOT molecule) thickness in the calculations and varied its thermal diffusivity χ. From very high values of χ down to that of octane, the radii obtained from best fits to data were identical (within 0.1 nm) to the ones determined without the AOT shell. If its χ was chosen significantly smaller than that of octane, the best fit radii started to deviate remarkably towards smaller values; but at the same time the temporal evolution was modified decreasing the overall fit quality. This statement also holds for the preliminary low-intensity data. So it may be concluded that the AOT shell does not provide some kind of thermal isolation, but allows for transfer of heat at least as well as n-octane. It will be interesting to study further micellar systems with other surfactants in order to look for possible nanoscopic thermal isolators. A final remark: the decay parameter $R^2/4\chi$ yields a value of 70 fs for the volume of a single water molecule (radius $\approx$0.2 nm); this is well compatible with the 500 fs equilibration time found in [14]. It will be an interesting aspect of future work to apply our technique to smaller aggregates down to the molecular scale looking, e.g., for information about specific molecular channels for heat transfer.

In summary, we have directly observed the ultrafast cooling process of nanometer-sized reverse micelles with picosecond pump-probe IR spectroscopy. The data can very well be described in terms of heat diffusion, where the thermal relaxation dynamics is completely governed by the radius of the water droplets. The ionic surfactant AOT obviously provides a good heat contact between water and nonpolar solvent, and overall the reverse micelles stand quite high transient temperatures (up to 100 °C). So our study shows a new way to measure the size of the aqueous core of reverse micelles, and can provide very special conditions to study chemical or biological reactions inside the confined water pool.

The authors thank D. Schwarzer for providing the analytical solution of the heat equation.

[1] H. Mays and G. Ilgenfritz, J. Chem. Soc. Faraday Trans. **92**, 3145 (1996).
[2] B. Farago *et al.,* Phys. Rev. Lett. **65**, 3348 (1990).
[3] T. Hellweg *et al.,* Phys. Rev. E **57**, 6825 (1998).
[4] L. Foret and A. Würger, Phys. Rev. Lett. **86**, 5930 (2001).
[5] Y. N. Cao *et al.,* J. Phys. Chem. B **101**, 3005 (1997).
[6] J. Faeder and B. M. Ladanyi, J. Phys. Chem. B **104**, 1033 (2000).
[7] M. Bey Temsamani *et al.,* J. Phys. Chem. B **102**, 3335 (1998).
[8] Q. Li, T. Li, and J. Wu, J. Phys. Chem. B **104**, 9011 (2000).
[9] M. D'Angelo *et al.,* Phys. Rev. E **54**, 993 (1996).
[10] D. Pant, R. E. Riter, and N. E. Levinger, J. Chem. Phys. **109**, 9995 (1998).
[11] C. A. S. D. S. Venables and K. Huang, J. Phys. Chem. B **105**, 9132 (2001).
[12] C. Borsarelli and S. E. Braslavsky, J. Phys. Chem. B **101**, 6036 (1997).
[13] S. Woutersen, U. Emmerichs, and H. J. Bakker, Science **278**, 658 (1997).
[14] A. J. Lock, S. Woutersen, and H. J. Bakker, J. Phys. Chem. A **105**, 1238 (2001).
[15] R. Laenen, C. Rauscher, and A. Laubereau, Phys. Rev. Lett. **80**, 2622 (1997).
[16] G. M. Gale *et al.,* Phys. Rev. Lett. **82**, 1068 (1999).
[17] J. Deak *et al.,* J. Phys. Chem. A **104**, 4866 (2000).
[18] T. Patzlaff *et al.,* Chem. Phys. **261**, 381 (2000).
[19] G. Seifert, T. Patzlaff, and H. Graener, Vib. Spectrosc. **23**, 219 (2000).
[20] *Structure and Reactivity in Reverse Micelles,* edited by M. P. Pileni (Elsevier, Amsterdam, 1989).
[21] H. R. Wyss and M. Falk, Can. J. Chem. **48**, 607 (1970).
[22] T. Iwata, J. Koshoubu, C. Jin, and Y. Okubo, Appl. Spectrosc. **51**, 1269 (1997).
[23] H. Graener *et al.,* J. Mol. Liq. **84**, 161 (2000).